Multi-Axis Attitude Control of Flexible Spacecraft Using Smart Structures and Hybrid Control Scheme

Morteza Shahravi, Milad Azimi

Department of mechanical engineering, Space Research Institute, Tehran, Iran
(e-mail: shahravi@ aut.ac.ir, azimi@mut.ac.ir)

Abstract: This paper presents a hybrid control design approach for simultaneous three axis attitude manoeuvre and active vibration suppression of a flexible spacecraft, in the presence of sensor noises and external bounded disturbances. The spacecraft considered as a rigid hub with two elastic appendages embedded with piezoelectric sensor/actuator patches. Using a modified sliding mode control by introducing a synthesized sliding manifold ensures that the spacecraft follows the shortest possible path to the desired orientation and highly reduce the switching action and excitation of flexible modes. A modified positive feedback scheme is developed to design a more symmetrical way to stabilize the vibration modes. Stability proof of the overall closed loop system is given via Lyapunov analysis. Numerical simulation results are presented to show the merit of this approach.

Keywords: Attitude Control, Active Vibration Control, Nonlinear Dynamics, Sliding Mode control, Smart Structures.

1. INTRODUCTION

Attitude slewing of spacecraft with flexible structural elements such as solar arrays, gravity gradient booms, antennas, and other light weight parts has received significant focus on providing the control effort for targeting flexible parts and tracking maneuver with simultaneous vibration suppression. In order to satisfy maneuver and pointing requirements (Zhang and Zeng, 2012), the interaction between both attitude and active vibration reduction controller's and structure should be handled carefully (Hyland et al., 1993; Junkins and Bang, 1993; Singhose et al., 1997). The dynamics of such flexible spacecraft involves the coupling of ODE for attitude dynamics and PDE for vibration of flexible appendages. This represented by a set of Hybrid Differential Equations of motion (HDE).

Control strategies have emerged for smoothly shaped maneuvers with vibration excited (Singh and Vadali, 1993). Also, the actual performance of controllers is highly sensitive to the error introduced by mathematical model simplification. Therefore the key issues can be classified into modeling error, control/structure interaction, robustness, and etc. There has been a lot of research and investigation effort for such problem. Numerical techniques have been reported with analysis and experimental verification. Accordingly, many researchers have surmounted by finite dimensional approximation of the original systems. Simultaneous attitude maneuver with vibration suppression has been considered by Vadali (Vadali et al., 1990). One of the most applicable and efficient control techniques is known to be Sliding Mode Control (SMC) which is suitable for systems with parameter uncertainties and nonlinear structure (Drakunov and Utkin, 1992; Hung et al., 1993). This technique has been reported in most of the previous studies, however the spacecraft flexible dynamics are considered as an external perturbation which is affected the rigid body motion (Hu and Ma, 2005a; Hu and Ma, 2005b; Shahravi and Kabganian, 2005; Shahravi et al., 2006). All the same, in previous works, for the case of three-axis attitude maneuver with nonlinear coupled rigid-flexible dynamics, the SMC approach has been modified by ignoring these nonlinear terms. The disadvantageous of these modification techniques lies in shifting of the calculated parameters away from what has happened in reality. Hu proposed a robust nonlinear SMC theory for 3-axis attitude control and vibration suppression of a flexible spacecraft simultaneously with parameter uncertainty and control saturation nonlinearity (Hu, 2009; Hu, 2010). Elsewhere the mentioned researcher et al. (Hu et al., 2008) used a control technique which incorporated both SMC and command input shaping for the vibration suppression of a flexible spacecraft in single axis maneuver without proof of global stability of the system. The classical sliding mode theory with disturbance accommodating control is combined for attitude tracking maneuver of spacecraft (Kim et al., 1998). A modified version of classical SMC called smoothing model-reference control is proposed by Lo and Chen in which the attitude tracking performance is increased without proof of global stability of the system (Lo and Chen, 1995).

The problem of residual vibrations control has received tremendous interest and poses a challenge task for spacecraft designers (Azadi et al., 2011; Hu, 2006). They suggested using smart materials such as shape memory alloys (SMA), Piezoelectric (PZT), and etc. for this problem. The PZT materials have the advantages of high stiffness, light weight, low power consumption, high frequency response and easy implementation. The global stability of the fully coupled nonlinear system has not been reported in these researches.

This paper presents a method for degrading the induced vibration and limiting the control action during the slew maneuver based on fully nonlinear dynamic model. The control of spacecraft for high precision pointing is formulated incorporating control of attitude by modified SMC (MSMC) and Strain Rate Feedback (SRF) techniques simultaneously. Global stability of the complete system has been guaranteed.

2. DYNAMIC MODELING

Figure 1 demonstrates the schematic of the hub with two flexible appendages. A spacecraft model with rigid main body and two clamped loaded Euler-Bernoulli beams bounding with PZT layers are considered to model the elastic deformations of the flexible parts in multi axis attitude maneuvers.

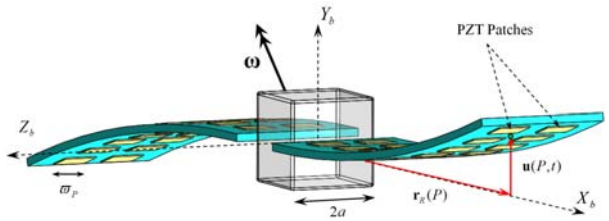

Fig. 1. Flexible spacecraft model.

The coordinates which used are shown in Figure 1, by choosing the center of the mass of the spacecraft as the body fixed reference frame origin $(O\,X\,Y\,Z)\big|_b$, the attitude motions may be decoupled from the translational motions. The beams have the same length L_b, thickness t_b, mass per unit length ρ_b, bending moment of inertia I_b and Young's modulus E_b. The PZT sensors/actuators patches with the length L_P, thickness h_p, mass per unit length ρ_p, bending moment of inertia I_p and Young's modulus E_p are bounded in both sides of each panel.

The kinematics between the body angular velocity and attitude parameter need to be established. The orientation of the body fixed coordinate $(O\,X\,Y\,Z)\big|_b$ with respect to an arbitrary inertial frame $(O\,X\,Y\,Z)\big|_I$ may be defined using orthonormal direction cosine $\mathbf{C}(t)\in\mathbf{R}^{3\times3}$ matrix (Shuster, 1993):

$$\left\{(O\;X\;Y\;\;Z)\big|_b\,(t)\right\}=\mathbf{C}(t)\left\{(t)\,(O\;X\;Y\;\;Z)\big|_b\,(t)\right\} \tag{1}$$

The unit quaternion which is a non-minimal representation of an object attitude, completely avoids singular orientations. A quaternion may be presented as a vector $\mathbf{q}=\begin{bmatrix}q_0 & \mathbf{q}_{1:3}\end{bmatrix}^T\in R_{4\times1}$ (Xiao et al., 2011), that is:

$$\begin{cases}\mathbf{q}_{1:3}=\begin{bmatrix}q_1 & q_2 & q_3\end{bmatrix}^T=e(t)\,Sin\left(\dfrac{\Phi(t)}{2}\right)\\ q_0=Cos\left(\dfrac{\Phi(t)}{2}\right)\end{cases}\quad 0\le\Phi(t)\le2\pi \tag{2}$$

where $\Phi(t)$ is a rotation of a rigid body about the principle Euler rotation axis $e(t)$. The time derivative of the unit quaternion is derived to calculate attitude at any moment:

$$\dot{q}(t)=\frac{1}{2}\begin{bmatrix}q_0\mathbf{I}_{3\times3}+{}^{\times}\mathbf{q}_{1:3} & -\mathbf{q}_{1:3}^T\end{bmatrix}^T\boldsymbol{\omega} \tag{3}$$

where ${}^{\times}\mathbf{q}_{1:3}$ is the skew-symmetric matrix of $\mathbf{q}_{1:3}$, and $\boldsymbol{\omega}=\omega_x X_b+\omega_y Y_b+\omega_z Z_b$ the body angular velocity of the spacecraft. The displacement $r_p(t)$ of any point p on the spacecraft can be defined as:

$$\mathbf{r}(P,t)=\mathbf{r}_R^i(P)X_b+\mathbf{u}^i(P,t)Y_b \tag{4}$$

where $\mathbf{r}_R^i(P)$ is a vector from center of the mass to the un-deformed point p, $\mathbf{u}^i(P,t)$, $i=1,2$ represents the elastic deflection p on ith appendage with respect to nominal position of point p. The velocity of a point p with respect to the body fixed reference frame can be obtained by differentiation of (4):

$$\mathbf{v}(p,t)=\dot{\mathbf{u}}^i(p,t)+\boldsymbol{\omega}\times\left(\mathbf{r}_R^i(P)+\mathbf{u}^i(P,t)\right) \tag{5}$$

The kinetic energy of the system including PZT patches can be expressed as:

$$T=\sum_{i=1}^{2}T_b^{\,i}+\sum_{i=1}^{2}\sum_{j=1}^{n_j}{}^jT_p^{\,i} \tag{6}$$

where T_b^i, T_P^i and n_j represents the kinetic energy of the main structure, the kinetic energy of the jth sensor/actuator pair and the number of PZT patches, respectively, and can be obtained as:

$$\begin{aligned}T_b^{\,i}=&\frac{1}{2}\int_S\rho_b\,\mathbf{v}(p,t).\mathbf{v}(p,t)dS=\\&\frac{1}{2}\boldsymbol{\omega}^T\mathbf{J}_b\boldsymbol{\omega}+\frac{1}{2}\sum_{i=1}^{2}\int_a^{a+L_b}\left(\rho_b^i\dot{\mathbf{u}}^i(p,t)^T\dot{\mathbf{u}}^i(p,t)\right)\\&+\boldsymbol{\omega}\left(\rho_b^i\left({}^{\times}\mathbf{r}_R^i(P)+{}^{\times}\mathbf{u}^i(P,t)\right)\dot{\mathbf{u}}^i(p,t)\right)dx\end{aligned} \tag{7}$$

$$\begin{aligned}T_P^{\,i}=&\frac{1}{2}\boldsymbol{\omega}^T\mathbf{J}_p\boldsymbol{\omega}+\frac{1}{2}\sum_{i=1}^{2}\sum_{j=1}^{n_j}\int_{x_i}^{x_i+L_P}{}^j\rho_P^i\,\dot{\mathbf{u}}^i(p,t)^T\dot{\mathbf{u}}^i(p,t)dx+\\&\frac{1}{2}\boldsymbol{\omega}\sum_{i=1}^{2}\sum_{j=1}^{n_j}\int_{x_i}^{x_i+L_P}{}^j\rho_P^i\left({}^{\times}\mathbf{r}_R^i(P)+{}^{\times}\mathbf{u}^i(P,t)\right)\dot{\mathbf{u}}^i(p,t)dx\end{aligned} \tag{8}$$

where $\mathbf{J}$ is the hub moment of inertia and x_i is starting x-coordinate of PZT patch. The potential energy of the flexible structure including PZT patches is considered as below:

$$V=\sum_{i=1}^{2}V_b^{\,i}+\sum_{i=1}^{2}\sum_{j=1}^{n_j}{}^jV_p^{\,i} \tag{9}$$

where V_b^i and ${}^jV_P^i$ are the potential energy of the ith main structure and the jth sensor/actuator pair respectively, and can be written as:

$$V_b^{\,i} = \frac{1}{2}\sum_{i=1}^{2}\int_{a}^{a+L_b} E_b^{\,i} I_b^{\,i}\left(\frac{\partial^2 \mathbf{u}^i(P,t)}{\partial x^2}\right)^2 dx \tag{10}$$

$$\begin{aligned} {}^jV_P^{\,i} = \frac{1}{2}\sum_{i=1}^{2}\sum_{j=1}^{n_j} {}^jE_P^{\,i}\left({}^j\varpi_p^{\,i}\,{}^jh_p^{\,i}\right)\left({}^jy^{\,i2} + {}^jy^{\,i}\,{}^jh_p^{\,i} + \frac{{}^jh_p^{\,i2}}{3}\right) \\ \int_{x_i}^{x_i+L_P}\left(\frac{\partial^2 \mathbf{u}^i(p,t)}{\partial x^2}\right)^2 dx \end{aligned} \tag{11}$$

where ${}^jy^{\,i}$ is the distance from starting point of PZT with respect to neutral axis of the beam and ${}^j\varpi_p^i$ is the width of the jth PZT layer. The virtual work done by the external torques and PZT patches is given by:

$$\delta W_{nc} = \delta W_T + \sum_{i=1}^{2}\sum_{j=1}^{n_j}\delta\,{}^jW_p^{\,i} \tag{12}$$

where $\delta\,{}^jW_p^{\,i}$ is the work done by the j-th PZT patch on i-th appendage and δW_T is the work done by the external control torque inputs and disturbances. The work done by the jth PZT patch is the combination of the conservative and non-conservative work terms, defined by integration over the volume of the PZT patches:

$$\delta\,{}^jW_p^{\,i} = \sum_{i=1}^{2}\sum_{j=1}^{n_j}\delta\,{}^jW_p^{\,i}\Big|_c + \sum_{i=1}^{2}\sum_{j=1}^{n_j}\delta\,{}^jW_p^{\,i}\Big|_{nc} \tag{13}$$

$${}^jW_p^{\,i} = \frac{1}{2}\,{}^j\varpi_p^i\sum_{i=1}^{2}\sum_{j=1}^{n_j}\int_{{}^jx^i}^{{}^jx^i+L_P}\int_{{}^jy^i}^{{}^jy^i+{}^jh_p^i}\begin{Bmatrix}{}^jE_3^{\,i}\\ {}^jS_1^{\,i}\end{Bmatrix}^T\begin{bmatrix}1 & 0\\ 0 & -1\end{bmatrix}\begin{Bmatrix}{}^jD_3^{\,i}\\ {}^jT_1^{\,i}\end{Bmatrix}dy\,dx \tag{14}$$

Using constitutive equation of PZT material (Meitzler et al., 1988) (See Appendix 1) and ${}^jS_1^i = -y(\partial^2\mathbf{u}(p,t)/\partial x^2)$, then (14) becomes:

$$\begin{aligned} W_p^{\,i} = \frac{1}{2}\,{}^j\varpi_p^i\sum_{i=1}^{2}\sum_{j=1}^{n_j}\int_{{}^jx^i}^{{}^jx^i+L_P}\int_{{}^jy^i}^{{}^jy^i+{}^jh_p^i}\left\{\left({}^j\varepsilon_3^{T\,i} - {}^jd_{31}^{\,i2}\,{}^jE_P^{\,i}\right){}^jE_3^{\,i2}\right\} \\ -{}^jE_P^{\,i}y\left(\left(2\,{}^jd_{31}^{\,i}\,{}^jE_3^{\,i}y\,\frac{\partial^2\mathbf{u}^i(p,t)}{\partial x^2}\right) - \left(\frac{\partial^2\mathbf{u}^i(p,t)}{\partial x^2}\right)^2\right)dy\,dx \end{aligned} \tag{15}$$

The last term of (15) expressed as PZT potential energy ${}^jV_P^i$. In other words the potential energy expression is composed of conservative works. The non-conservative work term is defined as follows:

$${}^jW_p^{\,i}\Big|_{nc} = \frac{1}{2}\,{}^j\xi_p^{\,i}\,{}^j\eta_p^{i2} - \left\{\mathbf{q}_k^i\right\}^T\left\{{}^j\Re_p^i\right\}{}^j\eta_p^i \tag{16}$$

with:

$${}^j\xi_p^{\,i} = \sum_{i=1}^{2}\sum_{j=1}^{n_j}\frac{{}^j\varpi_p^{\,i}L_P}{{}^jh_p^{\,i}}\left({}^j\varepsilon_3^{T\,i} - {}^jd_{31}^{\,i2}\,{}^jE_P^{\,i}\right)$$

$${}^j\eta_p^{\,i} = \sum_{i=1}^{2}\sum_{j=1}^{n_j}{}^jE_3^{\,i}\times{}^jh_p^{\,i} \tag{17}$$

$${}^j\Re_p^{\,i} = \sum_{i=1}^{2}\sum_{j=1}^{n_j}{}^jd_{31}^{\,i}\,{}^jE_P^{\,i}\,{}^j\varpi_p^{\,i}\left({}^jy^{\,i} + \frac{{}^jh_p^{\,i}}{2}\right)\int_{{}^jx^i}^{{}^jx^i+L_P}\left\{\boldsymbol{\psi}''(x)\right\}^T dx$$

where η_p^i is the electrode voltage, $\left\{\mathbf{q}_k^i\right\} = [q_1\,q_2\,\ldots\,q_n]$ is the kth generalized coordinates for ith appendage, and $\{\boldsymbol{\psi}(x)\}$ is the element shape function. Substituting (16) into (12), the total work can be expressed as:

$$W_{nc} = \frac{1}{2}\{\eta\}^T[\Im]\{\eta\} - \{q\}^T[R]\{\eta\} + W_T \tag{18}$$

where:

$$\begin{aligned} &[\Im] = diag\left({}^j\xi_p^{\,i}\right),\quad [R] = \left[\left\{{}^1\Re_p^i\right\}\left\{{}^2\Re_p^i\right\}\ldots\left\{{}^{n_j}\Re_p^i\right\}\right], \\ &\eta = \left[{}^1\eta_p^i\;\;{}^2\eta_p^i\;\ldots\;{}^{n_j}\eta_p^i\right]^T \end{aligned} \tag{19}$$

Utilizing Assumed Mode Method (AMM), the elastic deflections of the flexible substructures may be expressed as:

$$\mathbf{u}^i(x,t) = \sum_{k=1}^{m}{}^i\boldsymbol{\psi}_k^T(x)\,\mathbf{q}_k^i(t) = \{\psi\}\left\{\mathbf{q}\right\} \tag{20}$$

where $\mathbf{u}^i(x,t)$ is elastic displacement of ith appendage along x axis. The Lagrange equation of the motion in terms of quasi-coordinate in a vector form is a kind of dynamic control equation established by introducing dynamic functions, as presented below (Meirovitch, 1991):

$$\begin{cases}\dfrac{d}{dt}\left(\dfrac{\partial L}{\partial\boldsymbol{\omega}}\right) + {}^\times\boldsymbol{\omega}\dfrac{\partial L}{\partial\boldsymbol{\omega}} = \boldsymbol{\tau} + \mathbf{u}\\ \dfrac{d}{dt}\left(\dfrac{\partial L}{\partial\dot{\mathbf{q}}_k}\right) - \dfrac{\partial L}{\partial\mathbf{q}_k} = \mathbf{0}\end{cases} \tag{21}$$

where $\mathbf{u}\in\mathbf{R}^{3\times1}$ is the control torque inputs generated by actuators placed on rigid main body and $\boldsymbol{\tau}\in\mathbf{R}^{3\times1}$ is an external torque term representing the effect of external disturbances. Suppose that the energy dissipation occur via the structural damping and define Rayleigh's dissipation function as:

$$T_d = \frac{1}{2}\dot{\mathbf{q}}_k^T\mathbf{C}\dot{\mathbf{q}}_k \tag{22}$$

Inserting (6), (9), (12), and (22) into (21) and carrying out the indicated operations, the attitude dynamic model of a flexible spacecraft can be obtained in the following form:

$$\begin{aligned} &\begin{bmatrix}\mathbf{M}_{RR} & \mathbf{M}_{RF}\\ \mathbf{M}_{FR} & \mathbf{M}_{FF}\end{bmatrix}\cdot\begin{Bmatrix}\dot{\boldsymbol{\omega}}\\ \ddot{\mathbf{q}}_k\end{Bmatrix} + \begin{Bmatrix}\mathbf{f}_R\left(\boldsymbol{\omega},\dot{\mathbf{q}}_k,\mathbf{q}_k\right)\\ \mathbf{f}_F\left(\boldsymbol{\omega},\dot{\mathbf{q}}_k,\mathbf{q}_k\right)\end{Bmatrix} = \begin{Bmatrix}\boldsymbol{\tau}+\mathbf{u}\\ -[R][g_a]\{\eta_a\}\end{Bmatrix} \\ &\{\eta_S\} = [g_s][\Im]^{-1}[R]^T\left\{\mathbf{q}_k\right\} \end{aligned} \tag{23}$$

where $[g_s]$ and $[g_a]$ are the PZT sensor/actuator amplifier gains. The elements of sub matrices M and f are given in Appendix 2. The PZT patches will be used as sensors and actuators; accordingly they will have voltage inputs and outputs. As it can be seen from (23), $[R]$ and $[\Im]$ matrices can be decomposed into sensor and actuator parts corresponding to the sensor/actuator voltages, $\{\eta_S\}$ and $\{\eta_a\}$.

3. CONTROLLER DESIGN

In the present work, three-axis attitude maneuver and vibration control is considered. The quaternions are chosen for representation of the attitude of the spacecraft. By taking angular velocity and quaternion vectors, a modified sliding manifold being proposed as:

$$\mathbf{S} = \boldsymbol{\omega}_e + \mathbf{K}\tanh(q_{0-e})\mathbf{q}_{1:3-e} \tag{24}$$

where $\boldsymbol{\omega}_e = \boldsymbol{\omega} - \boldsymbol{\omega}_d$ is the spacecraft angular velocity tracking error, and $\mathbf{q}_e = \mathbf{q}\langle\times\rangle\mathbf{q}_d^{-1}$ is the quaternion tracking error, in which $\langle\times\rangle$ is the quaternion products, $\mathbf{q}_d$ and $\boldsymbol{\omega}_d$ are the desired quaternion and angular velocity, respectively.

Theorem 1. The control objective is to stabilize the flexible spacecraft by forcing the rigid body modes to follow some desired trajectories, while simultaneously reduce the elastic modes. The desired attitude maneuver with high mode flexibility can be realized, if the sliding condition $\dot{V} \prec 0$ is satisfied.

Proof: The desired state that slides on the sliding surface can be shown to be asymptotically stable by choosing the candidate Lyapunov function as:

$$V = \frac{1}{2}\mathbf{S}^T\mathbf{M}_{RR}\mathbf{S} \tag{25}$$

The proposed Lyapunov function is valid since it vanishes at equilibrium point $\mathbf{S} = \mathbf{0}$ and is globally positive definite for $\mathbf{S} \neq \mathbf{0}$ since $\mathbf{M}_{RR}$ is positive definite. The time derivative of Lyapunov function is given by:

$$\dot{V} = \mathbf{S}^T\mathbf{M}_{RR}\dot{\mathbf{S}} \tag{26}$$

where the derivative of the sliding surface is defined as:

$$\dot{\mathbf{S}} = \dot{\boldsymbol{\omega}}_e + \mathbf{K}\tanh(q_{0-e})\dot{\mathbf{q}}_{1:3-e} \tag{27}$$

From the equation of the motion we have:

$$\mathbf{M}_{RR}\dot{\boldsymbol{\omega}} = \left\{-\mathbf{M}_{RF}\ddot{\underset{\sim}{\mathbf{q}}}_k - \mathbf{f}_R\left(\boldsymbol{\omega}, \dot{\underset{\sim}{\mathbf{q}}}_k, \underset{\sim}{\mathbf{q}}_k\right)\right\} + (\mathbf{u} + \boldsymbol{\tau}) \tag{28}$$

Multiply each side of (27) by $\mathbf{M}_{RR}$ combined with (28) leads to the following expression for $\dot{V}$:

$$\begin{aligned}\dot{V} = {} & \mathbf{S}^T\left[\left\{-\mathbf{M}_{RF}\ddot{\underset{\sim}{\mathbf{q}}}_k - \mathbf{f}_R\left(\boldsymbol{\omega}, \dot{\underset{\sim}{\mathbf{q}}}_k, \underset{\sim}{\mathbf{q}}_k\right) + \boldsymbol{\tau}\right\}\right] \\ & + (\mathbf{u}) + \left(K_1\tanh(q_{0-e})\mathbf{M}_{RR}\dot{\mathbf{q}}_{1:3-e}\right)\end{aligned} \tag{29}$$

The controller designed by the sliding mode approach consists of two different tasks. First one is to define an appropriate sliding surface and the other one is to improve the sliding condition, commands the states remain on the sliding surface. By solving the above equation for the control input, the external control torque can be derived in such a way that:

$$\mathbf{u} = \mathbf{u}_{eq} + \mathbf{u}_{VS} \tag{30}$$

where the variable structure and equivalent parts of controller input defined as:

$$\mathbf{u}_{VS} = -\left(K_2\mathbf{S}(t)\right) - \left(K_3\tanh\left(\frac{\mathbf{S}(t)}{P^2}\right)\right) \tag{31}$$

$$\begin{aligned}\mathbf{u}_{eq} = {} & \left\{\mathbf{M}_{RF}\ddot{\underset{\sim}{\mathbf{q}}}_k + \mathbf{f}_R\left(\boldsymbol{\omega}, \dot{\underset{\sim}{\mathbf{q}}}_k, \underset{\sim}{\mathbf{q}}_k\right) - \boldsymbol{\tau}\right\} \\ & - \left(K_1\tanh(q_{0-e})\mathbf{M}_{RR}\dot{\mathbf{q}}_{1:3-e}\right)\end{aligned} \tag{32}$$

Substitutions of (31) and (32) into the sliding condition yields:

$$\dot{V} = -\mathbf{S}^T(t)\left\{\left(K_2\mathbf{S}(t)\right) + \left(K_3\tanh\left(\frac{\mathbf{S}(t)}{P^2}\right)\right)\right\} \prec 0 \tag{33}$$

where K_n with $n = 1,2,3$ are positive definite matrices, and P^2 is a scalar sharpness function that regulates the control action rates. Note that the term $\dot{\mathbf{q}}_{1:3-e}$ in (32), introduces nonlinear terms in sliding mode controller. The equivalent control $\mathbf{u}_{eq}$ part turns the sliding surface $\mathbf{S}(t)$ into an invariant manifold for the system, to ensure that $\dot{\mathbf{S}} = 0$. Whereas the variable structure part $\mathbf{u}_{VS}$, is chosen to ensure that the $\mathbf{S} = 0$, thus the designing surface is attractive and the desired condition can be reached in finite time. In other words, this implies from theorem and the K_n values that the control objective $[\mathbf{q} \quad \boldsymbol{\omega}]_d^T = [1 \quad \mathbf{0}_{1\times3} \quad \mathbf{0}_{1\times3}]^T$ is accessible, as $t \to \infty$ and the asymptotic global stability can be achieved due to the negative definite $\dot{V} = -0.5\mathbf{S}^T\mathbf{u}_{VS}$.

It can be seen from (31) and (32) that the stability and robustness of controller performance guaranteed if the upper bounds of the perturbations are known. This knowledge may cause the controller produce the over-conservative high gain K_3. This may cause chattering phenomenon. In order to overcome with this source of degradation or over action, the hyperbolic tangent function is used to reduce chattering. It should be mentioned that, in practical implementation $\boldsymbol{\tau}$ can be eliminated from $\mathbf{u}_{eq}$ provided $K_3 \succ \|\boldsymbol{\tau}\|$ in $\mathbf{u}_{VS}$ to guarantee robust and stable control performance.

Also, the active vibration suppression system using the PZT sensor and actuator can be actively suppressed the solar and environmental induced vibration to the flexible appendages during attitude maneuver. Since no external field is applied to the sensor layer, the electric displacement developed on the sensor surface is directly proportional to the strain acting on it. Also, piezoelectric materials can be used as strain rate

sensors. The output current of the PZT sensor measures the moment rate of the flexible appendages. This current is converted into the open circuit sensor voltage V_S using a signal conditioning device with the gain G_C and applied to an actuator with a suitable controller gain. Thus, the sensor output voltage is obtained as:

$$V_S(t)=G_C\, i(t)=G_C\, e_{31}\left(\frac{h_b}{2}+h_p\right)\varpi_p\int_0^{L_p}\frac{\partial^2}{\partial x^2}\psi_k(x)\dot{q}_k(t)dx \quad (34)$$

where $i(t)$ is the circuit current. This sensor voltage is given as input to the controller and the output of the controller is the controller gain multiplied by the sensor voltage. Thus, the input voltage to the actuator V_a, in other word the controller input $\bar{u}(t)$ is given by:

$$V_a(t)=\bar{u}(t)=\mathbf{K}_p\times V_S(t) \quad (35)$$

where $\mathbf{K}_p$ is the controller gain matrix. Note that feedback gain matrix $\mathbf{K}_p$ consists of each feedback gain, which is associated with each flexible PZT patch. The actuator equation is derived from the converse piezoelectric equation and the relative control force $\mathbf{f}_{ctrl}$ produced by the actuator that is applied on the appendages is obtained using bending moment theory:

$$\mathbf{f}_{ctrl}=E_P\, d_{31}\,\varpi_p\left(\frac{h_P+h_b}{2}\right)\int_0^{L_p}\frac{\partial}{\partial x}\psi_k(x)dx\,V_a(t) \quad (36)$$

where d_{31} is the PZT strain constant.

4. NUMERICAL SIMULATIONS AND RESULTS

Simulation of fully nonlinear 3-axis attitude maneuver of a flexible spacecraft has been carried out using MATLAB/SIMULINK software to demonstrate the performance of the proposed approach. The proposed control system objective of a flexible spacecraft model is to reduce the induced vibration and tracking a target in sample mission. This can be perform using smart materials for active vibration control with SRF technique and modified SMC method using prevalent actuators such as Control Moment Gyros (CMGs), reaction wheels, thrusters and magnetorquers, as shown in Appendix 3 (Figure 10). Also the proposed method enables attitude targeting in the presence of bounded disturbances and sensor noises. This is done in order to examine the robustness of the proposed controller. The attitude sensors noises and the external disturbances used in the simulation are $0.0002(\mathbf{S})$ and $\boldsymbol{\tau}(t)=0.01\big(0.02\sin(0.01t)+0.03\cos(0.015t)\big)+\big(0.1\sin(0.01t)\times 0.1\cos(0.01t)\big)$, respectively.

The desired maneuver is 160° slew with simultaneous vibration suppression. This is usually a fast and large angle maneuver. The numerical values of the parameters used in the simulation study are presented in table 1. The initial conditions for the angular velocity are set to $\boldsymbol{\omega}(t_0)=\begin{bmatrix}0 & 0 & 0\end{bmatrix}^T$ and for quaternion parameters are given by $\mathbf{q}(t_0)=\begin{bmatrix}0.174 & -0.263 & 0.789 & -0.526\end{bmatrix}^T$. The first three flexible modes are retained in the model for discretization of elastic deformations. For control implementation, design parameters are considered as $\mathbf{K}_1=0.21\mathbf{I}_{3\times3}$, $\mathbf{K}_2=6\mathbf{I}_{3\times3}$ and $\mathbf{K}_3=0.001\mathbf{I}_{3\times3}$.

Table 1. Parameters of flexible spacecraft.

Parameters	Flexible appendage	Piezoelectric Layer
Young's Modulus (GPa)	$E=39.72$	$E_p=68$
Density (kg/m)	$\rho_b=1.51$	$\rho_p=2.31$
Thickness (m)	$t_b=0.02$	$t_p=0.00035$
Width (m)	$b=0.5$	$b=0.08$
Length (m)	$L_b=2$	$L_p=0.08$
PZT Strain Constant (m/V)	-	$d_{31}=125\times10^{-12}$
PZT Stress Constant (Vm/N)	-	$e_{31}=10.5\times10^{-3}$
Hub dimension (m)	$a=0.3$	
Spacecraft moment of inertia (kg.m^2)	$\begin{bmatrix}7.31 & 0 & 0\\ 0 & 13.44 & 0\\ 0 & 0 & 11.72\end{bmatrix}$	

Dynamical behaviors of the controlled system are shown in Figs 2-9. Smoothness and convergence of attitude error in terms of quaternions and angular rate are shown in Figs. 2 and 3. Figures 4(a)-4(c) and 5 show the required control torques for different states. As shown in these figures, the flexible structures shows significant coupling with the structural dynamics. Moreover, the input control torque u_z (Fig. 4(c)) about the in-plane motion of the elastic appendages shows significant coupling with the structural dynamics. This makes sense, of the governing equations describe such a dynamic phenomenon. The $\mathrm{sgn}(.)$ term present in the conventional sliding surface design is replaced by a hyperbolic tangent function in order to reduce the effects of chattering.

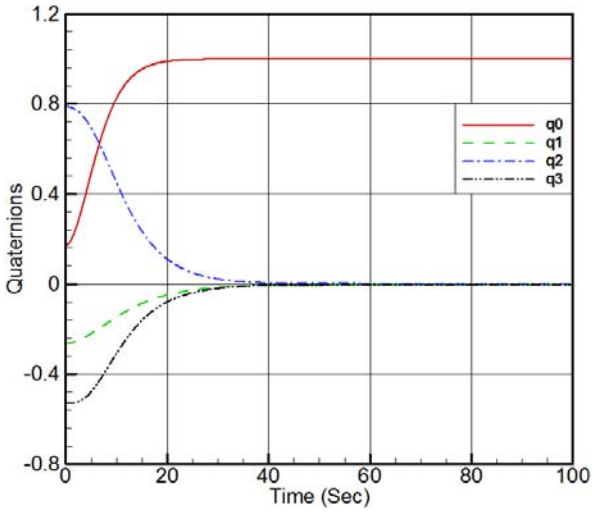

Fig. 2. Time history of attitude quaternions.

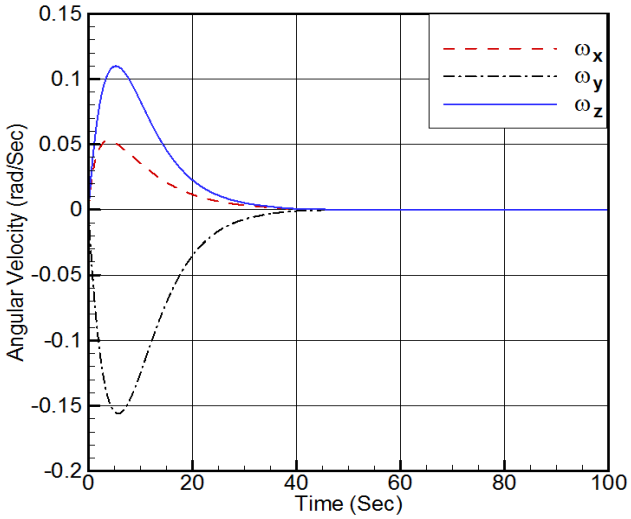

Fig. 3. Time history of angular velocity.

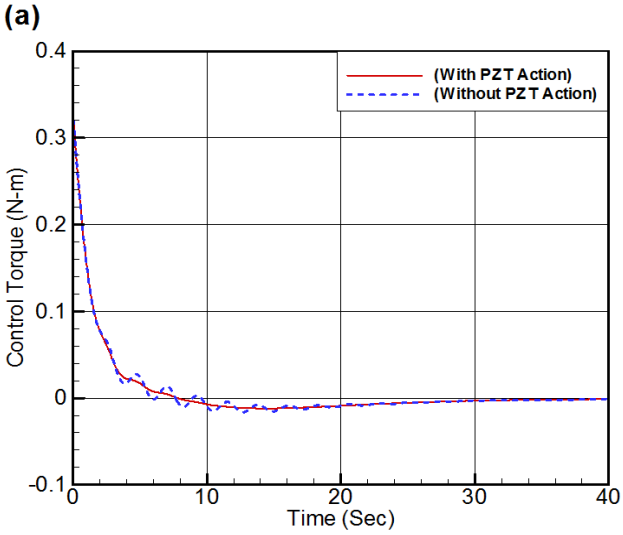

Fig. 4(a). Time history of control torque (u_x) with and w/o active vibration suppression.

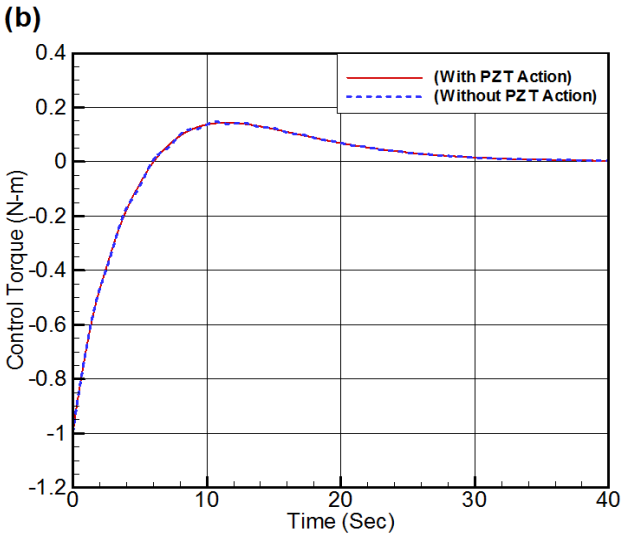

Fig. 4(b). Time history of control torque (u_y) with and w/o active vibration suppression.

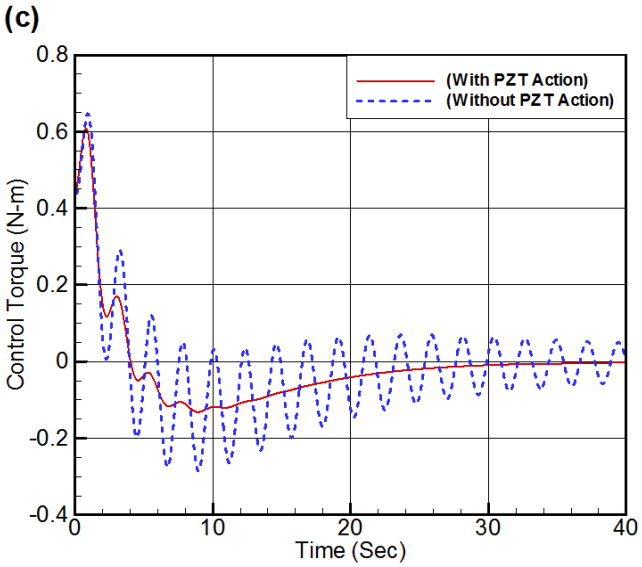

Fig. 4(c). Time history of control torque (u_z) with and w/o active vibration suppression.

For comparison, the system is also controlled by using sliding mode control designed in conventional form (CSMC), which it has been investigated extensively.

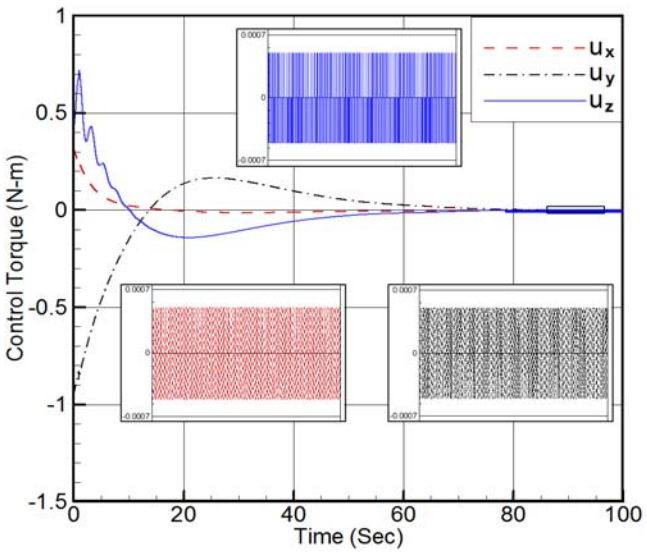

Fig. 5. Time history of control torque using conventional (Not-modified) SMC.

As shown in Fig. 5, using conventional SMC (without modification) causes steady state error arising from flexible mode excitation. Also, active suppression of the structural vibration causes smooth and fine actuation of attitude controller. This is an important characteristic for actual implementation of the controller. Convergence of the flexible body coordinates and PZT actuation voltage are shown in Figs. 6-9. From the comparison of Figure 8(a) with Figure 8(b), it can be deduced that the effect of PZT actions is noteworthy. Furthermore, the simulation results in Figures 8(a) and 8(b) shows that the tip deflection response using modified SMC leads to better performance compared to the case with CSMC approach.

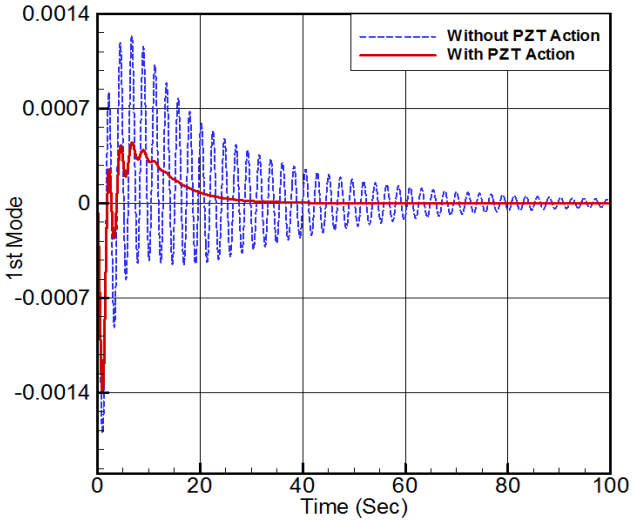

Fig. 6. Time history of 1st vibrational mode.

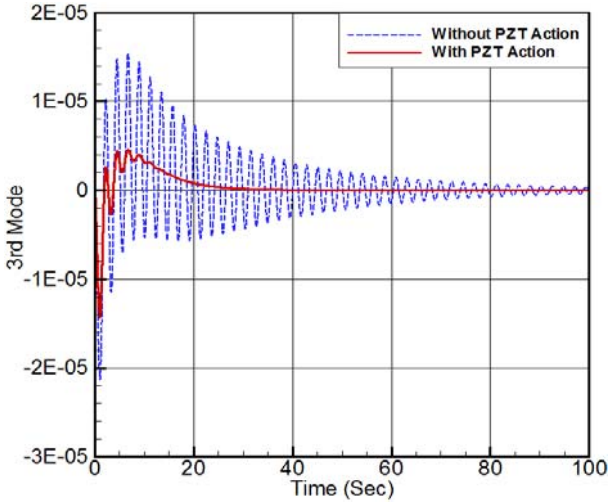

Fig. 7. Time history of 3rd vibrational mode.

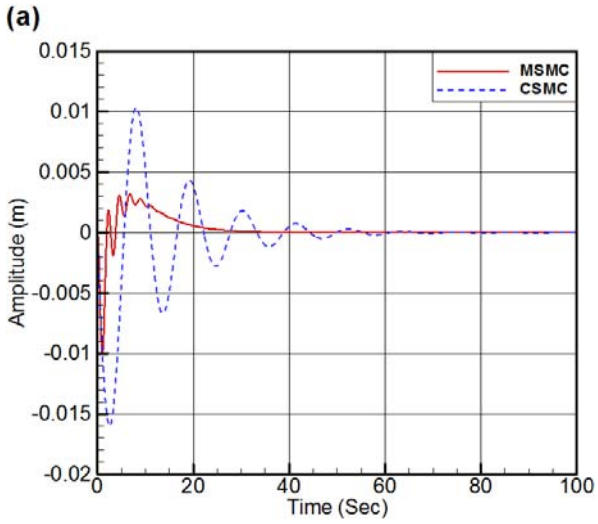

Fig. 8 (a). Tip deflection response of the appendage with active vibration suppression.

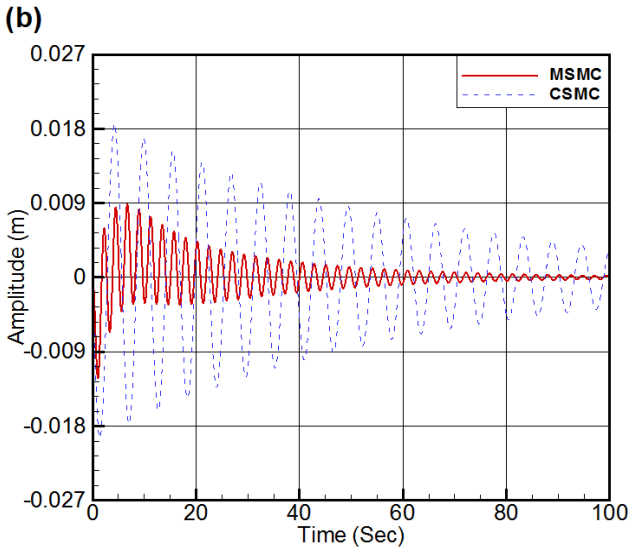

Fig. 8 (b). Tip deflection response of the appendage w/o active vibration suppression.

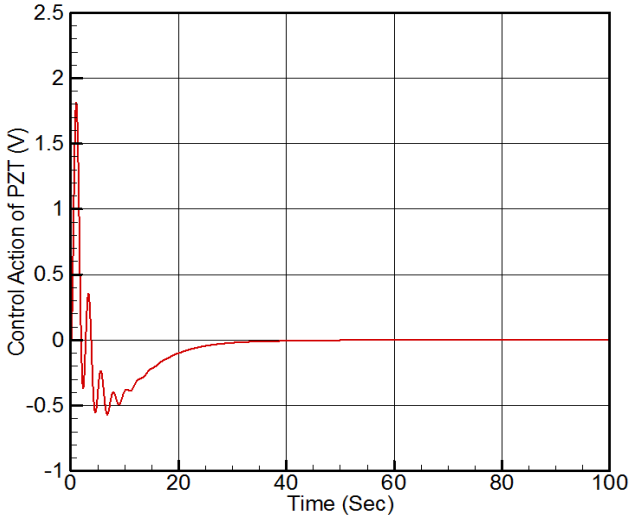

Fig. 9. Time history of PZT actuation voltage.

Extensive simulations were also done using different values of the system parameters in order to ensure the merit of the proposed scheme in various conditions.

5. CONCLUSIONS

A new approach based on the modified sliding mode control and active vibration control technique using piezoceramics as actuator/sensor was proposed for the control of large angle multi-axis attitude maneuver of the flexible spacecraft. The control purpose was achieved using two tasks, one targeting the attitude maneuver as soon as possible, and the other, controlling the induced structural vibration. The design of the attitude controller was based on sliding mode control theory using a synthesized hybrid sliding surface and hyperbolic tangent switching function. The advantage of application of this control law is that once the desired orientation is attained in the shortest time without vast excitation of the elastic modes and resonance of the spacecraft flexible structure. It was shown that the proposed scheme is an effective approach

in comparison with the conventional sliding mode control and traditional composite algorithm for fast targeting and suppression of structural vibration and also, is robust against the external disturbances and noises. The future research directions include the digital implementation of the control scheme on hardware platforms for attitude control experimentation.

REFERENCES

Azadi, M., Fazelzadeh, S., EghtesaD, M. & Azadi, E. 2011. Vibration suppression and adaptive-robust control of a smart flexible satellite with three axes maneuvering. *Acta Astronautica,* 69**,** 307-322.

Drakunov, S. V. & Utkin, V. 1992. Sliding mode control in dynamic systems. *International Journal of Control,* 55**,** 1029-1037.

Hu, Q.-L., Wang, Z. & Gao, H. 2008. Sliding mode and shaped input vibration control of flexible systems. *Aerospace and Electronic Systems, IEEE Transactions on,* 44**,** 503-519.

Hu, Q. 2009. Variable structure maneuvering control with time-varying sliding surface and active vibration damping of flexible spacecraft with input saturation. *Acta Astronautica,* 64**,** 1085-1108.

Hu, Q. 2010. Sliding mode attitude control with L_2-gain performance and vibration reduction of flexible spacecraft with actuator dynamics. *Acta Astronautica,* 67**,** 572-583.

Hu, Q. & Ma, G. 2005a. Variable structure control and active vibration suppression of flexible spacecraft during attitude maneuver. *Aerospace Science and Technology,* 9**,** 307-317.

Hu, Q. & Ma, G. 2005b. Vibration suppression of flexible spacecraft during attitude maneuvers. *Journal of guidance, control, and dynamics,* 28**,** 377-380.

Hu, Q. L., Ma, G.F. 2006. Optimal sliding mode maneuvering control and active vibration reduction of flexible spacecraft. *Proceedings of the Institution of Mechanical Engineers, Part G, Journal of Aerospace Engineering,* 220**,** 317-35.

Hung, J. Y., Gao, W. & Hung, J. C. 1993. Variable structure control: a survey. *Industrial Electronics, IEEE Transactions on,* 40**,** 2-22.

Hyland, D., Junkins, J. & Longman, R. 1993. Active control technology for large space structures. *Journal of Guidance, Control, and Dynamics,* 16**,** 801-821.

Junkins, J. L. & Bang, H. 1993. Maneuver and vibration control of hybrid coordinate systems using Lyapunov stability theory. *Journal of guidance, control, and dynamics,* 16**,** 668-676.

Kim, J. & Crassidis, J. L. 1998. Disturbance accommodating sliding mode controller for spacecraft attitude maneuvers. *Advances in the Astronautical Sciences,* 100**,** 141-154.

Lo, S.-C. & Chen, Y.-P. 1995. Smooth sliding-mode control for spacecraft attitude tracking maneuvers. *Journal of Guidance, Control, and Dynamics,* 18**,** 1345-1349.

Meirovitch, L. 1991. Hybrid state equations of motion for flexible bodies in terms of quasi-coordinates. *Journal of Guidance, Control, and Dynamics,* 14**,** 1008-1013.

Meitzler, A., Tiersten, H., Warner, A., Berlincourt, D., Couqin, G. & Welsh III, F. 1988. IEEE standard on piezoelectricity. Society.

Shahravi, M. & Kabganian, M. Attitude tracking and vibration suppression of flexible spacecraft using implicit adaptive control law. American Control Conference, 2005. Proceedings of the 2005, 2005. IEEE, 913-918.

Shahravi, M., Kabganian, M. & Alasty, A. 2006. Adaptive robust attitude control of a flexible spacecraft. *International Journal of Robust and Nonlinear Control,* 16**,** 287-302.

Shuster, M. D. 1993. A survey of attitude representations. *Navigation,* 8**,** 9.

Singh, T. & Vadali, S. 1993. Input-shaped control of three-dimensional maneuvers of flexible spacecraft. *Journal of guidance, control, and dynamics,* 16**,** 1061-1068.

Singhose, W. E., Banerjee, A. K. & Seering, W. P. 1997. Slewing flexible spacecraft with deflection-limiting input shaping. *Journal of Guidance, Control, and Dynamics,* 20**,** 291-298.

Vadali, S., Junkins, J. & Byers, R. 1990. Near-minimum time, closed-loop slewing of flexible spacecraft. *Journal of Guidance, Control, and Dynamics,* 13**,** 57-65.

Xiao, B., Hu, Q. & Ma, G. 2011. Adaptive quaternion-based output feedback control for flexible spacecraft attitude tracking with input constraints. *Proceedings of the Institution of Mechanical Engineers, Part I: Journal of Systems and Control Engineering,* 225**,** 226-240.

Zhang, X. & Zeng, M. 2012. Multi-objective control of spacecraft attitude maneuver based on Takagi-Sugeno fuzzy model. *Journal of Control Engineering and Applied Informatics,* 14**,** 31-36.

APPENDIX A

The 3D constitutive equation for a piezoelectric element can be shown to have the following standard notation (Meitzler et al., 1988):

$$\begin{bmatrix} \underline{D_i} \\ \underline{S_j} \end{bmatrix} = \begin{bmatrix} \underline{\varepsilon_i^T} & \underline{d_{ij}^1} & \underline{d_{ij}^2} \\ \underline{d_{ij}^{1T}} & \underline{S_{ij}^{E1}} & \underline{0} \\ \underline{d_{ij}^2} & \underline{0} & \underline{S_{ij}^{E2}} \end{bmatrix} \begin{bmatrix} \underline{E_i} \\ \underline{T_j} \end{bmatrix} \tag{37}$$

where $S_i \ (i = 1,...,6)$ is the strain, $D_i \ (i = 1,2,3)$ is the electric charge density displacement, $E_i \ (i = 1,2,3)$ is the electrical field strength, $\sigma_i \ (i = 1,...,6)$ is the stress, $\underline{\varepsilon_i^T} \ (i = 1,2,3)$, $\underline{S_{ij}^{Ek}} (i = 1,5, \ j = 1,2,3,5, \ k = 1,2)$ and $d_{ij}^k \ (i = 1,3, j = 1,3,5, k = 1,2)$ are permittivity, elastic compliance and piezoelectricity (strain) coefficient constants of the PZT material, respectively.

$$\underline{\varepsilon_i^T} = \begin{bmatrix} \varepsilon_1^T & 0 & 0 \\ 0 & \varepsilon_1^T & 0 \\ 0 & 0 & \varepsilon_3^T \end{bmatrix}, \underline{d_{ij}^1} = \begin{bmatrix} 0 & 0 & 0 \\ 0 & 0 & 0 \\ d_{31} & d_{31} & d_{33} \end{bmatrix},$$
$$\underline{d_{ij}^2} = \begin{bmatrix} 0 & d_{15} & 0 \\ d_{15} & 0 & 0 \\ 0 & 0 & 0 \end{bmatrix} \tag{38}$$

$$\underline{S_{ij}^{E1}} = \begin{bmatrix} S_{11}^E & S_{12}^E & S_{13}^E \\ S_{12}^E & S_{11}^E & S_{13}^E \\ S_{13}^E & S_{13}^E & S_{13}^E \end{bmatrix}, \underline{S_{ij}^{E2}} = \begin{bmatrix} S_{55}^E & 0 & 0 \\ 0 & S_{55}^E & 0 \\ 0 & 0 & S_{55}^E \end{bmatrix} \tag{39}$$

The strain condition based on Euler-Bernoulli beam theory is defined as:

$$\varepsilon_x = -y\frac{\partial^2 w}{\partial x^2}, \varepsilon_y = \varepsilon_z = \gamma_{xy} = \gamma = \gamma_{yx} = 0 \tag{40}$$

It can be seen from (40) that the (37) reduced to 1-D constitutive equation of PZT material:

$$\begin{Bmatrix} D_3 \\ S_1 \end{Bmatrix} = \begin{bmatrix} \varepsilon_3^T & d_{31} \\ d_{31} & S_{11}^E \end{bmatrix} \begin{Bmatrix} E_3 \\ T_1 \end{Bmatrix} \tag{41}$$

Using the fact that $S_{ij}^E = E_P^{-1}$, (41) can be expressed as below:

$$\begin{Bmatrix} D_3 \\ T_1 \end{Bmatrix} = \begin{bmatrix} \varepsilon_3^T - d_{31}^2 E_P & d_{31} E_P \\ -E_P d_{31} & E_P \end{bmatrix} \begin{Bmatrix} E_3 \\ S_1 \end{Bmatrix} \tag{42}$$

APPENDIX B

$$\mathbf{J} = \mathbf{J}_h + \mathbf{J}_b + \mathbf{J}_p = \left[J^{ij} \right]_{3\times 3} \tag{43}$$

$$J^{11} = I_{XX} + \sum_{i=1}^{2} \int_a^{a+L_b} \rho_b^i \, {}^i\mathbf{u}^2 dx + \sum_{i=1}^{2} \sum_{j=1}^{n_j} \int_{x_i}^{x_i+L_P} {}^j\rho_P^i \, {}^i\mathbf{u}^2 dx \tag{44}$$

$$J^{12} = J^{21} = -\sum_{i=1}^{2} \int_a^{a+L_b} \rho_b^i \, {}^i\mathbf{u} dx + \sum_{i=1}^{2} \sum_{j=1}^{n_j} \int_{x_i}^{x_i+L_P} {}^j\rho_P^i \, {}^i\mathbf{u} \, dx \tag{45}$$

$$J^{13} = J^{31} = 0, \quad J^{22} = I_{YY}, \quad J^{23} = J^{32} = 0 \tag{46}$$

$$J^{33} = I_{ZZ} + \sum_{i=1}^{2} \int_a^{a+L_b} \rho_b^i \, {}^i\mathbf{u}^2 dx + \sum_{i=1}^{2} \sum_{j=1}^{N_j} \int_{x_i}^{x_i+L_{Pi}} {}^j\rho_P^i \, {}^i\mathbf{u}^2 dx \tag{47}$$

$$\mathbf{M}_{RR} = \left[M_{RR}^{ij} \right]_{3\times 3} \tag{48}$$

$$M_{RR}^{11} = I_{XX} + \sum_{i=1}^{2} \left\{ \begin{array}{l} {}^i\mathbf{q}_k^T \, {}^i\Upsilon_{yy} \, {}^i\mathbf{q}_k + {}^ia_y \left(\rho_b + \sum_{j=1}^{N_j} {}^j\rho_P \right) \\ +2 \, {}^ia_y \, {}^i\Upsilon_y^T \, {}^i\mathbf{q}_k \end{array} \right\} \tag{49}$$

$$M_{RR}^{12} = M_{RR}^{21} = -\sum_{i=1}^{2} \left\{ \begin{array}{l} {}^i\Upsilon_{yx}^T \, {}^i\mathbf{q}_k + {}^ia_x \, {}^ia_y + {}^ia_x \, {}^i\Upsilon_{yy}^T \, {}^i\mathbf{q}_k \\ +{}^ia_y \left(\rho_b \frac{L_b^2}{2} + \sum_{j=1}^{N_j} {}^j\rho_P \frac{{}^jL_P^2}{2} \right) \end{array} \right\} \tag{50}$$

$$M_{RR}^{13} = M_{RR}^{31} = 0, \quad M_{RR}^{22} = I_{YY}, \quad M_{RR}^{23} = M_{RR}^{32} = 0 \tag{51}$$

$$M_{RR}^{33} = I_{ZZ} + \sum_{i=1}^{2} \left\{ {}^i\mathbf{q}_k^T \, {}^i\Upsilon_{yy} \, {}^i\mathbf{q}_k + {}^ia_y^2 \left(\rho_b + \sum_{j=1}^{N_j} {}^j\rho_P \right) \right\} + \left\{ 2 \, {}^ia_y \, {}^i\Upsilon_y^T \, {}^i\mathbf{q}_k + \rho_b \int_0^{L_b} x^2 dx + \sum_{j=1}^{N_j} {}^j\rho_P \int_{x_i}^{x_i+L_P} x^2 dx \right\} \tag{52}$$

$$\mathbf{M}_{RF} = \mathbf{M}_{RF} = \left[{}^1a_x \quad {}^2a_x \right] \begin{bmatrix} {}^1\Upsilon_y^T & \mathbf{0} \\ \mathbf{0} & {}^2\Upsilon_y^T \end{bmatrix} - \left[{}^1\Upsilon_{yx}^T \quad {}^2\Upsilon_{yx}^T \right] \tag{53}$$

$$\mathbf{M}_{FF} = \begin{bmatrix} {}^1\Upsilon_{yy} & \mathbf{0} \\ \mathbf{0} & {}^2\Upsilon_{yy} \end{bmatrix} \tag{54}$$

$$\mathbf{f}_R = \left[f_R^{ij} \right]_{3\times 1} \tag{55}$$

$$f_R^{11} = \omega_x \omega_z \sum_{i=1}^{2} \left\{ \begin{array}{l} {}^i\Upsilon_{yx}^T \, {}^i\mathbf{q}_k + {}^ia_x \, {}^ia_y + {}^ia_x \, {}^i\Upsilon_y^T \, {}^i\mathbf{q}_k \\ +{}^ia_y \left(\rho_b \frac{L_b^2}{2} + \sum_{j=1}^{N_j} {}^j\rho_P \frac{{}^jL_P^2}{2} \right) \end{array} \right\} + \omega_y \omega_z \left\{ \begin{array}{l} {}^i\mathbf{q}_k^T \, {}^i\Upsilon_{yy}^T \, {}^i\mathbf{q}_k + {}^ia_y^2 \left(\rho_b + \sum_{j=1}^{N_j} {}^j\rho_P \right) \\ +2a_y \left(\rho_b + \sum_{j=1}^{N_j} {}^j\rho_P \right) {}^i\Upsilon_y^T \, {}^i\mathbf{q}_k \end{array} \right\} + 2\omega_x \left\{ {}^i\dot{\mathbf{q}}_k^T \, {}^i\Upsilon_{yy}^T \, {}^i\mathbf{q}_k + {}^ia_y \, {}^i\Upsilon_y^T \, {}^i\dot{\mathbf{q}}_k \right\} + \omega_y \omega_z \left(I_{ZZ} - I_{yy} \right) \tag{56}$$

$$f_R^{21} = \omega_z \omega_y \sum_{i=1}^{2} \left\{ \begin{array}{l} {}^i\Upsilon_{yx}^T \, {}^i\mathbf{q}_k + {}^ia_x \, {}^ia_y + {}^ia_x \, {}^i\Upsilon_y^T \, {}^i\mathbf{q}_k \\ +{}^ia_y \left(\rho_b \frac{L_b^2}{2} + \sum_{j=1}^{N_j} {}^j\rho_P \frac{{}^jL_P^2}{2} \right) \end{array} \right\} + -2\omega_x \sum_{i=1}^{2} \left\{ {}^i\Upsilon_{yx}^T \, {}^i\dot{\mathbf{q}}_k + {}^ia_x \, {}^i\Upsilon_y^T \, {}^i\dot{\mathbf{q}}_k \right\} + \omega_x \omega_z \left(I_{XX} - I_{yy} \right) \tag{57}$$

$$f_R^{31} = -\left(\omega_x^2 - \omega_y^2 \right) \sum_{i=1}^{2} \left\{ \begin{array}{l} {}^i\Upsilon_{yx}^T \, {}^i\mathbf{q}_k + {}^ia_x \, {}^ia_y + {}^ia_x \, {}^i\Upsilon_y^T \, {}^i\mathbf{q}_k \\ +{}^ia_y \left(\rho_b \frac{L_b^2}{2} + \sum_{j=1}^{N_j} {}^j\rho_P \frac{{}^jL_P^2}{2} \right) \end{array} \right\} - \omega_x \omega_y \left\{ \begin{array}{l} {}^i\mathbf{q}_k^T \, {}^i\Upsilon_{yy}^T \, {}^i\mathbf{q}_k + {}^ia_y^2 \left(\rho_b + \sum_{j=1}^{N_j} {}^j\rho_P \right) \\ +2a_y \left(\rho_b + \sum_{j=1}^{N_j} {}^j\rho_P \right) {}^i\Upsilon_y^T \, {}^i\mathbf{q}_k \end{array} \right\} + 2\omega_z \left\{ {}^i\dot{\mathbf{q}}_k^T \, {}^i\Upsilon_{yx}^T \, {}^i\dot{\mathbf{q}}_k + {}^ia_x \, {}^i\Upsilon_y^T \, {}^i\dot{\mathbf{q}}_k \right\} + \omega_y \omega_x \left(I_{YY} - I_{XX} \right) \tag{58}$$

$$\mathbf{f}_F = \begin{bmatrix} {}^1\wp & \mathbf{0} \\ \mathbf{0} & {}^2\wp \end{bmatrix} {}^i\underset{\sim}{\mathbf{q}}_k + \omega_x \omega_y \left\{ \begin{bmatrix} {}^1\Upsilon_{xy} \\ {}^2\Upsilon_{xy} \end{bmatrix}^T \begin{bmatrix} {}^1\Upsilon_y & \mathbf{0} \\ \mathbf{0} & {}^2\Upsilon_y \end{bmatrix} \begin{bmatrix} {}^1a_x \\ {}^2a_x \end{bmatrix} \right\}$$
$$-\left(\omega_x^2 + \omega_z^2\right) \left\{ \begin{bmatrix} {}^1\Upsilon_{yy} & \mathbf{0} \\ \mathbf{0} & {}^2\Upsilon_{yy} \end{bmatrix} {}^i\underset{\sim}{\mathbf{q}}_k + \begin{bmatrix} {}^1\Upsilon_y & \mathbf{0} \\ \mathbf{0} & {}^2\Upsilon_y \end{bmatrix} \begin{bmatrix} {}^1a_x \\ {}^2a_x \end{bmatrix} \right\} \tag{59}$$

$${}^i\Upsilon_{yy} = \int_0^{L_b} \rho_b \, {}^i\boldsymbol{\psi}(x) \, {}^i\boldsymbol{\psi}^T(x) dx + \sum_{j=1}^{N_j} \int_{x_i}^{x_i + L_P} {}^j\rho_P \, {}^i\boldsymbol{\psi}(x) \, {}^i\boldsymbol{\psi}^T(x) dx \tag{60}$$

$${}^i\Upsilon_y = \int_0^{L_b} \rho_b \, {}^i\boldsymbol{\psi}(x) dx + \sum_{j=1}^{N_j} \int_{x_i}^{x_i + L_P} {}^j\rho_P \, {}^i\boldsymbol{\psi}(x) dx \tag{61}$$

$${}^i\Upsilon_{yx} = \int_0^{L_b} \rho_b \, {}^i\boldsymbol{\psi}(x) x \, dx + \sum_{j=1}^{N_j} \int_{x_i}^{x_i + L_P} {}^j\rho_P \, {}^i\boldsymbol{\psi}(x) x \, dx \tag{62}$$

$${}^i\wp = \sum_{j=1}^{n_j} {}^jE_P^i \left({}^j\varpi_p^i \, {}^jh_p^i \right) \left({}^jy^{i\,2} + {}^jy^i \, {}^jh_p^i + \frac{{}^jh_p^{i\,2}}{3} \right) \int_{x_i}^{x_i + L_P} \left(\frac{\partial^2 \boldsymbol{\psi}^i(x)}{\partial x^2} \right)^2 dx \times$$
$$+ \int_0^{L_b} E_b^i I_b^i \left(\frac{\partial^2 \boldsymbol{\psi}^i(x)}{\partial x^2} \right)^2 dx \tag{63}$$

APPENDIX C

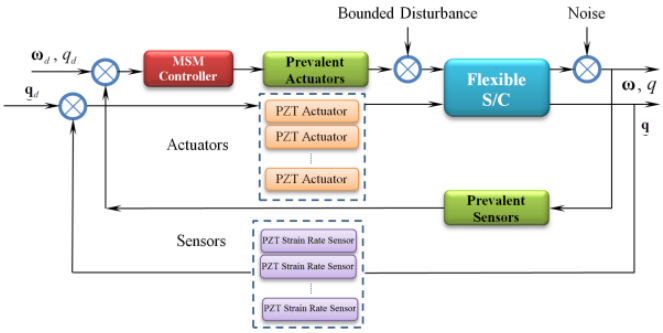

Fig. 10. Simulation model (MATLAB/SIMULINK).